DFT Atomic-Scale Insight into Pt/Cu Single Atom Alloy Clusters Supported on γ-Al2O3: The Effect of Hydrogen Environment

Masoud Shahrokhi, Tzonka Mineva, Abdennour Benabbas, Catherine Especel, Anthony Le Valant, Christian Ricolleau, Guillaume Wang, Jaysen Nelayah, Florence Epron, Hazar Guesmi

ChemCatChem

Research Article
doi.org/10.1002/cctc.202400565

Chemistry Europe
European Chemical Societies Publishing

www.chemcatchem.org

DFT Atomic-Scale Insight into Pt/Cu Single Atom Alloy Clusters Supported on γ-Al_2O_3: The Effect of Hydrogen Environment

Masoud Shahrokhi,*[a] Tzonka Mineva,[a] Abdennour Benabbas,[b] Catherine Especel,[b] Anthony Le Valant,[b] Christian Ricolleau,[c] Guillaume Wang,[c] Jaysen Nelayah,[c] Florence Epron,[b] and Hazar Guesmi*[a]

Single atom alloy (SAA) clusters formed by anchoring single atoms in small supported host clusters are emerging as catalysts with high performance. In this work, density functional theory (DFT) calculations and ab-initio molecular dynamics (AIMD) simulations are performed to study the stability and the structure evolution of γ-alumina-supported platinum/copper SAA clusters of sub-nanometer size in hydrogen environment. Due to the strong dynamic nature of both Cu cluster and anchored Pt single atom and their evolving interaction with the support, different isomers with different geometric and energetic properties are predicted. Extensive sampling through AIMD simulations reveals strong effect of hydrogen on the location of Pt single atom and strong variation of the cluster shape, evolving from 3D to concave and planar shapes wetting the alumina support. Interfacial site location of Pt single atom is found to be hydrogen coverage dependent. When the hydrogen coverage increases, the Pt single atom located preferentially at the interfacial site is pulled up by hydrogen atoms toward the upper surface Cu layers. The interaction of Pt/Cu cluster with alumina is predicted to decrease with increasing hydrogen coverage. Finally, electronic structure analysis reveals dramatic effect of hydrogen on the metallic nature of the catalysts.

Introduction

Sub-nanometer transition-metal (TM) clusters composed of few atoms have received significant attention because of their unique electronic, physical, and chemical properties that are different from their bulk analogues.[1] In heterogeneous catalysis, thanks to their specific molecular-like electronic structure and the high accessibility of their low coordinated surface atoms, several TM clusters are reported to exhibit exceptional catalytic activity in many reactions.[2,3] For instance, improved catalytic performance of sub-nanometer Cu clusters are found in the chemo-selective hydrogenation of olefins and carbonyl groups[4] and in C–C, C–N, C–O, C–S, and C–P bond forming reactions.[5] For Pt clusters of sub-nanometer size, superior activity is shown in the oxygen reduction reaction[6] and in the oxidative dehydrogenation reaction of alkanes.[7] Vajda *et al.* reported that Pt clusters of 8–10 atoms supported on high-surface-area alumina are 40–100 times more active for the oxidative dehydrogenation of propane than conventional Pt particles catalysts.[7] From DFT results, these authors explained the observed superior C–H activation originating from under-coordinated surface Pt sites. However, Pt suffers from low selectivity towards propylene and it is well known that the presence of Pt surface ensembles or at least two neighboring Pt surface sites may induce undesired side reactions such as hydrogenolysis, isomerization and coke formation.[8]

In order to overcome this problem and to achieve high selectivity while maintaining high activity during hydrogenation or dehydrogenation reactions, isolated Pt atoms were anchored in the surface layer of more inert host metals to form Pt single atom alloys (SAAs)[9–10] such as Pt/Ni,[9] Pt/Cu,[10] Pt/Sn,[11] Pt/Zn,[12] Pt/Ga[13] and Pt/In.[14] Among these systems, Pt/Cu SAAs are reported to achieve the desired high activity and selectivity for propane dehydrogenation reaction (PDH).[10] Sykes and coworkers[15] are the first to demonstrate how single Pt atom in Pt/Cu SAA catalysts may activate C–H bonds while the presence of Cu atoms prevents C–C cracking. Regarding the selectivity, the introduction of Cu downshifts the *d*-band center of surface Pt atoms which lowers the binding strength of propylene, promotes its desorption and results in higher propylene selectivity.[16] Moreover, based on DFT calculations on extended surface models[17] and Kinetic Monte Carlo (KMC) simulations,[10] Gong and coworkers suggested that the Pt/Cu SAA catalysts can break

[a] *Dr. M. Shahrokhi, Dr. T. Mineva, Dr. H. Guesmi*
ICGM, University Montpellier, CNRS, ENSCM
1919 Rte de Mende, 34293 Montpellier Cedex 5, France
E-mail: shahrokhimasoud37@gmail.com
hazar.guesmi@umontpellier.fr

[b] *A. Benabbas, Prof. C. Especel, Dr. A. Le Valant, Dr. F. Epron*
CNRS, Université de Poitiers, Institut de Chimie des Milieux et des Matériaux de Poitiers (IC2MP), F-86000 Poitiers, France

[c] *Prof. C. Ricolleau, Dr. G. Wang, Dr. J. Nelayah*
Université Paris Cité, CNRS, Laboratoire Matériaux et Phénomènes Quantiques
10 rue Alice Domon et Léonie Duquet, 75013 Paris, France

Supporting information for this article is available on the WWW under https://doi.org/10.1002/cctc.202400565

the scaling relationship by promoting the selectivity of propene, while maintaining reasonable PDH activity. However, questions remain open regarding these debated scaling relationships as quantum-molecular level investigations and analysis of these materials are still limited to simplified model extended surfaces and/or unsupported, gas-phase nanoparticles.[15,18] Furthermore, the interactions with the gas environment and oxide supports are scarcely considered. It is widely recognized that exposure to reductive[19,20] or oxidative atmospheres[21,22] can significantly alter the stability[23] and morphology of supported clusters, including atomic segregation and atomic diffusion behaviors.[24,25] Thus, ignoring these changes may lead to inaccuracies in predicted properties.[26] To gain atomic-scale insight into Pt/Cu SAA clusters, we investigate in this work the stability and reactivity of $Cu_{12}Pt_1$ clusters supported on alumina. In addition, as hydrogen is ubiquitous in many de/hydrogenation reactions, the effect of adsorbed hydrogen atoms on the geometric, energetic and electronic structures of SAA clusters, supported on γ-Al_2O_3(100) surface, is analyzed. Finally, the thermodynamic phase diagram of Pt/Cu/γ-Al_2O_3(100) SAA cluster toward hydrogen pressure is evaluated and the electronic structure analysis is undertaken for the critical domains.

Results and Discussion

Structure and Stability of Cu_{13} and $Cu_{12}Pt_1$ Clusters Supported on γ-Alumina Surface

Computational studies based on classical interatomic potentials indicate that 3D geometries are the preferred ground state structures of free Cu_{13} clusters,[27,28] while ab-initio calculations predict the stability of bilayered structures.[29,30] As a first structural investigation, we performed DFT optimization calculations of these two competitive Cu cluster structures of 13 atoms deposited on γ-Al_2O_3(100) surface. The results indicate a superior stability by ~0.3 eV for the 3D compact structure (Figure S1), where copper atoms are arranged in a tight triangular bonding network with an average Cu–Cu bond length of 2.43 Å. This length is 5% shorter than the distance between first neighbors in the bulk Cu structure.[31] The calculated interaction energies with the alumina support (Eq. (4), see theoretical details) predict stronger chemical bonding of the compact cluster (−6.65 eV) compared to the bilayered one (−4.35 eV). This predicted favorable configuration was used as an initial structure in the velocity-scaled AIMD simulation, using the Born-Oppenheimer MD approach, at temperature (T) of 723 K, and 4000 steps (20 ps) trajectory length for an efficient sampling of the configurational space. Eight competitive structures at the lowest potential energy (Figure S2) were selected from AIMD trajectory and then quenched at 0 K by performing DFT geometry optimization calculations. Finally, the most energetically favorable quenched structure of γ-Al_2O_3 supported Cu_{13} was used to study the stability and the preferable location of anchored Pt single atom.

Figure 1a shows the three considered locations of Pt single atom in the Cu supported cluster: the top position ($Cu_{12}Pt_1$@top), the interfacial position in direct connection with the alumina support ($Cu_{12}Pt_1$@interface), and at the second layer position in between the top and interfacial positions ($Cu_{12}Pt_1$@2ndlayer). The DFT optimization calculations of the three supported $Cu_{12}Pt_1$ structures show the preference of Pt atom to be located close to the oxide support, $Cu_{12}Pt_1$@2ndlayer (0.0 eV) and $Cu_{12}Pt_1$@interface (+0.02 eV). The $Cu_{12}Pt_1$@top configuration is found to be less favorable by about +0.24 eV. To examine the impact of temperature on the structure of the catalyst and to explore the configurational space more thoroughly, the three minimum energy configurations were employed as initial guesses in further AIMD simulations at 723 K.

Figures 1b, 1c and 1d report the potential energy evolution during the AIMD simulations of the three supported $Cu_{12}Pt_1$clusters. Fourteen configurations of isomers selected at the lowest potential energies were again quenched at 0 K by means of DFT optimizations. This explorative study reveals a competitive stability of supported $Cu_{12}Pt_1$@interface (0.00 eV) and $Cu_{12}Pt_1$@2ndlayer (+0.13 eV) clusters with slight preference to the structures with Pt single atom located at the interfacial position, directly interacting with alumina support. The minimum energy configurations selected for $Cu_{12}Pt_1$@top clusters were predicted to be less stable by more than +0.3 eV. The analysis of the projected density of states (PDOSs) for the 5-*d* band of Pt atoms in the three investigated positions (Figure 2a) reveals notable disparities in the positions of the *d*-band centers relative to the Fermi level. Specifically, the *d*-band centers of Pt at the interfacial (−1.95 eV) and 2nd layer (−2.04 eV) positions exhibit significant shifts away from the Fermi level in comparison to the *d*-band center of Pt situated at the top site (−1.36 eV). This result suggests that the proximity of the Pt single atom to the alumina support might decrease its affinity towards the adsorbates. Notably, the *d*-band model indicates that, as the distance between the *d*-band center and the Fermi level increases, there is a decrease in the proportion of empty antibonding states. This phenomenon weakens the metal's propensity to bind with adsorbates.[32,33]

Moreover, the comparison of the PDOSs of Cu in Cu_{13} and in $Cu_{12}Pt_1$@interface shows a significant shift of the 3-*d* band center toward the Fermi level (+0.58 eV) when Pt is anchored in the cluster (see Figure 2a). Bader charge analysis also shows charge transfer from the positively charged Cu atoms to the negatively charged Pt atom. The charge transfer toward Pt can be rationalized in view of the Pauling electronegativity (χ) scale as Pt is the more electronegative atom with $\chi = 2.28$ compared to $\chi = 1.90$ for Cu. These results reveal the strong effect of alloying Cu cluster by Pt and predict an enhancement of the reactivity of the copper cluster.

The energetic analyses of the predicted most stable configuration, $Cu_{12}Pt_1$@interface (structure that will be considered subsequently in this study), shows an increase in the interaction energy between the metallic cluster and the support by about 11 eV compared to the pure Cu cluster. This increased interaction is concomitant with a pronounced accumulation of electron charge at the Pt interface site, as depicted in the density charge difference plot presented in Figure 2b. Bader charge analysis indicates a small charge transfer (0.012e) from

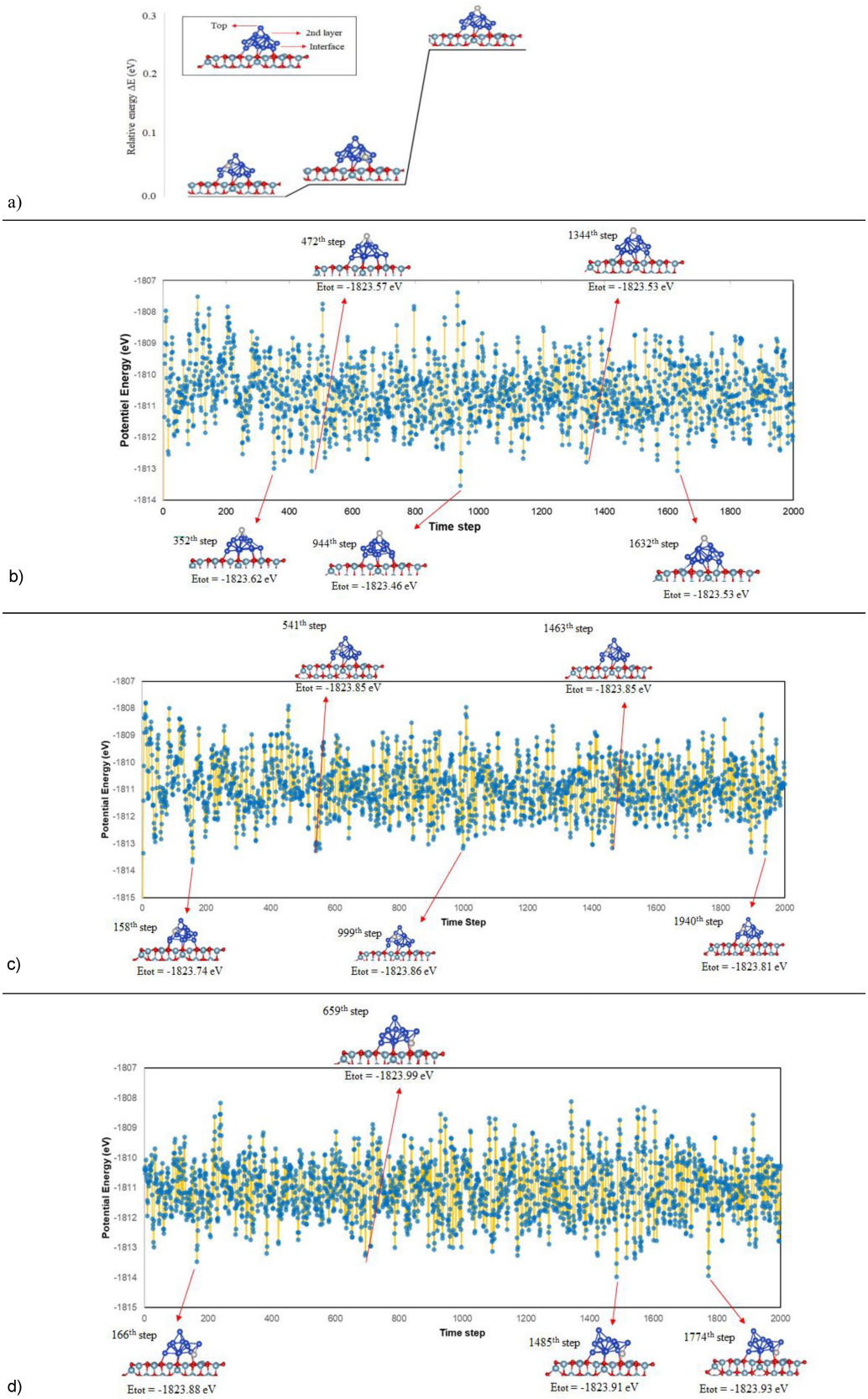

Figure 1. a) Lateral view of the three considered positions of Pt anchored in $Cu_{13}/\gamma\text{-}Al_2O_3(100)$. b), c) and d) Potential energy evolution as a function of time steps during velocity-scaled molecular dynamics calculations for $Cu_{12}Pt_1/Al_2O_3$ system for the three-considered positions of Pt. The simulation was conducted at a temperature of 723 K, and the total duration of the simulation was 20 ps. Fourteen lowest potential energy structures (PES) were extracted and quenched at 0 K by performing DFT optimizations. These structures are depicted in the figure along with their corresponding total energies after geometry optimization. Dark blue, light blue, red and white balls represent Cu, Al, O and Pt atoms, respectively.

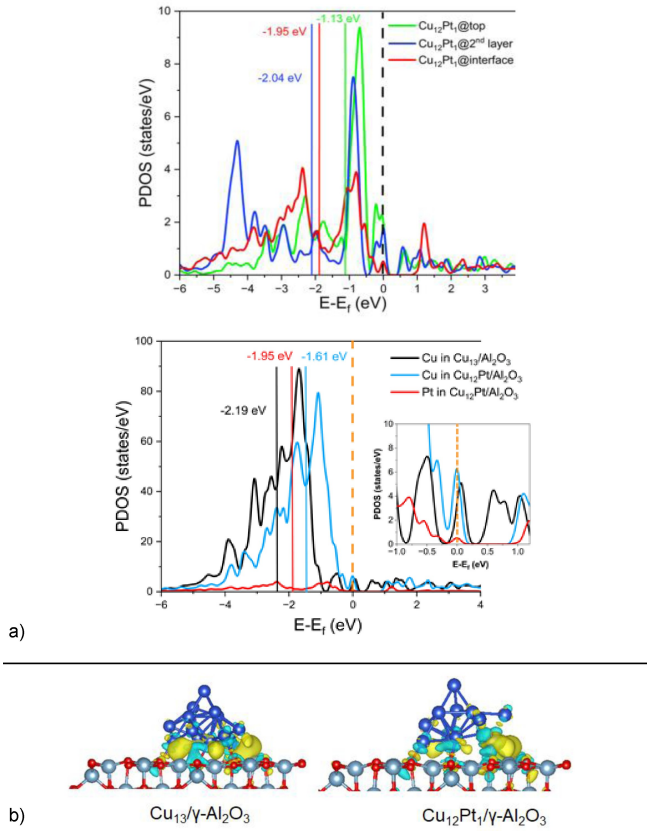

Figure 2. a) Projected density of state (PDOS) of (top) 5*d*-bands of Pt single atom anchored in different positions of the supported $Cu_{12}Pt_1$ clusters: top, 2nd layer and interfacial sites and (down) 3*d*-bands of Cu in supported Cu_{13} and in $Cu_{12}Pt_1$@interface clusters (the 5*d*-band of Pt atom (red curve) is also reported for comparison). The dashed lines represent the Fermi energy level and the straight lines with indicated values correspond to the position of the *d*-band centers. b) Charge density difference $\Delta\rho = \rho$ (cluster/γ-Al_2O_3) $-\rho$ (γ-Al_2O_3) $-\rho$ (cluster). $\Delta\rho$ is illustrated by iso-surfaces bounding regions of electron accumulation at $+0.0035$ e/Å^3 (yellow) and electron depletion at -0.0035 e/Å^3 (cyan). Dark blue, light blue, red and white balls represent Cu, Al, O and Pt atoms, respectively.

the $Cu_{12}Pt_1$@interface cluster to the support. The transfer of charge to Al atoms of the support is nearly negligible, consistent with the weak Lewis acid character of Al^{3+} on the γ-Al_2O_3(100) surface. In their recent investigation, Sautet et al.[34] thoroughly examined the electronic structure of interactions within small Pt clusters containing 8 atoms, supported on both α-Al_2O_3(0001) and γ-Al_2O_3(100) surfaces. They revealed bonding interactions between Pt and Lewis acidic Al^{3+} sites, alongside the Pt–O interaction. This phenomenon was notably pronounced on α-Al_2O_3(0001) surfaces but inexistent on γ-Al_2O_3(100) surfaces, which is in line with our analysis.

Adsorption of Hydrogen at Low Coverage

In contrast to symmetrical extended surfaces, small metallic clusters, especially alloyed clusters, may exhibit a diverse array of adsorption sites. Figure 3 reports seven configurations of γ-alumina supported $Cu_{12}Pt_1$@interface refined structure where hydrogen is adsorbed in different surface sites (top Cu, top Pt, bridge Cu–Pt, bridge Cu–Cu etc..). Considering the structures, one can expect, that the sharp-corner Cu atom, characterized by poor overlap between its 4 s orbital and the orbitals of neighboring atoms, would be more prone to hydrogen atom adsorption. However, contrary to this expectation, the adsorption on the top of the sharp-corner Cu atom is predicted to be highly endothermic (see Table S1). Moreover, the adsorption on Cu four-fold and three-fold sites that may offer a maximum of interactions to the hydrogen atom with the surface, are also found to be highly endothermic (see Table S1). The most favorable sites for hydrogen atom adsorption are identified as the bridge sites, where hydrogen adsorbs over two Cu–Cu atoms, and over an interfacial Pt and Al atoms. This is illustrated by configurations (e) and (f) in Figure 3a, respectively. Slight superiority is found for the adsorption on Cu sites, which may be linked to the *d*-band center analysis detailed in the previous section.

To evaluate the effect of temperature on the structure of the cluster and the adsorption site of H atom, the configuration (e) was used as a guess for molecular dynamics simulation. After 10 ps of simulation time, several low potential energy structures were quenched and optimized, leading to a minimum energy configuration with hydrogen adsorbed over Cu–Cu bridge site. In this configuration (Figure 3b), Cu–H bond was found to be of 1.64 Å and adsorption energy of -0.35 eV. This chemisorption gives rise to considerable structural change for the small $Cu_{12}Pt_1$ cluster, which again evidences the importance of this theoretical calculation procedure to identify refined structures.

The recently published work by K. Gu *et al.*[35] reported calculated adsorption energies per hydrogen atom on various H-adsorbed Pt/Cu(111) surfaces. According to their findings, the most stable configuration for the adsorption of a single H atom is at the top site of Pt, exhibiting an adsorption energy of -0.30 eV. This value is 0.05 eV lower than the calculated value on the Pt/Cu cluster in this study.

Furthermore, utilizing machine-learning accelerated molecular dynamics calculations grounded in density functional theory, these authors conclude that the adsorbed H atom that tends to be primarily located near the top site of the single Pt atom, potentially leads to its deactivation.[35] Consequently, the fact that hydrogen does not persist on the Pt interfacial site in the investigated $Cu_{12}Pt_1$@interface may suggest that the cluster is less susceptible to deactivation under low hydrogen coverage. This result will be further explored under conditions of high hydrogen coverage.

Adsorption of Hydrogen at High Coverage

The refined structure of alumina supported $Cu_{12}Pt_1$@interface cluster with one hydrogen atom was used as initial guess to study the adsorption of increasing number of hydrogen atoms. The same AIMD procedure was used to identify the stable configuration for a given hydrogen coverage (see Figure S3). The hydrogen coverage was calculated by defining the number of hydrogen atoms normalized by 13, which corresponds to the

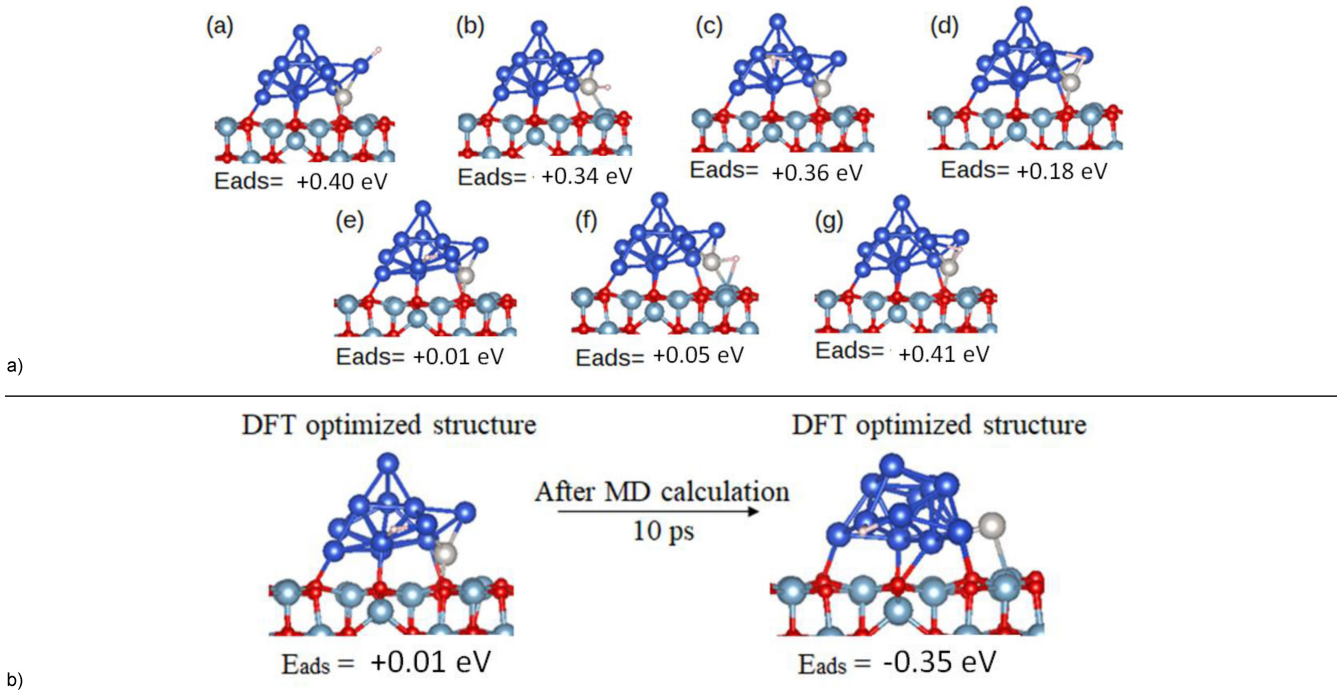

Figure 3. (a) Side views of the most stable structures for an atomic hydrogen adsorption on $Cu_{12}Pt_1/\gamma\text{-}Al_2O_3$ system in different positions. The adsorption energy values are calculated following the Eq. (1). (b) The configuration (e) showing a weak adsorption of H atom, was used as a guess for molecular dynamics simulation. After 10 ps of simulation time at T = 723 K, the minimum energy structure in the PES was quenched at 0 K giving the optimised structure with $E_{ads}H$ = -0.35 eV. Dark blue, light blue, red and white balls represent Cu, Al, O and Pt atoms, respectively. The small white ball represents adsorbed H.

number of atoms in the cluster. Therefore, $Cu_{12}Pt_1H_{14}$ represents the cluster fully covered by hydrogen (1.08 ML). In Figure 4 the identified minimum energy structures and their energetic and electronic features are reported.

The results indicate that hydrogen binding significantly influences the morphology and properties of the metallic cluster (Figure 4a). Typically, hydrogen atoms adsorb on the cluster's surface, with a preference for the bridge Cu–Cu and Cu–Pt sites. Adsorption on the top site is observed exclusively over the single Pt atom. The adsorption of hydrogen on the (100) alumina support and the formation of hydroxyl groups are found to be unfavorable. Furthermore, our molecular dynamics (MD) simulations indicate that no hydrogen spillover from the cluster to the support occurs across the range of hydrogen coverages studied. This observation aligns with the findings of Feng *et al.*,[36] who reported a hydrogen spillover process from hydroxylated $\gamma\text{-}Al_2O_3(110)$ surface to Cu cluster, while observing the absence of the reversed process.

To determine the average adsorption energy per H_2 molecule on $\gamma\text{-}Al_2O_3$ supported $Cu_{12}Pt_1$ clusters, we defined the simultaneous dissociative adsorptions of several H_2 molecules following Eq. (2) (See theoretical details). In Figure 4b, the evolution of the computed adsorption energies as a function of the hydrogen coverage are reported and compared to those on flat Cu(111), Pt(111) and PtCu(111) surfaces. As expected, the average adsorption energy on supported small clusters is predicted to be more exothermic compared to flat pure and alloyed Cu surfaces, and even surpasses that on pure Pt surfaces. This is attributed to the inherent metastability of these small-sized clusters compared to infinite surfaces. Additionally, their strong fluxionality allows them to adapt their shape upon adsorption. This behavior has been previously demonstrated in the context of H adsorption on various transition metal clusters, such as Pt/Al_2O_3,[37] $Pt–Sn/Al_2O_3$,[19,38] CuAu,[19,20] and Cu[36] clusters.

The computed adsorption energy depicted in Figure 4b reveals several evolution behaviors.Thus, fromtwo up to six adsorbed hydrogen atoms, the adsorption energy curve shows sharp fluctuations, which diminish with increasing the H-coverage. Then, monotonous decrease in adsorption energy is predicted for hydrogen coverage above 0.5 ML. The significant energy variation (−0.7 eV, −1.23 eV, −0.95 eV, and −1.2 eV for one, two, four, and six adsorbed H atoms, respectively) is likely a result of more pronounced morphological changes in the cluster, particularly with moderate hydrogen coverage.

As illustrated by the snapshots depicted in Figure 4a, four phase transitions of the supported $Cu_{12}Pt_1$ cluster occurred as the hydrogen coverage increases. After the initial phase leading to the bilayered structure, the cluster experiences significant elongation by more than 2 Å in the presence of hydrogen. During this second phase, exemplified by the $Cu_{12}Pt_1H_4$ and $Cu_{12}Pt_1H_6$ structures corresponding to coverages of 0.30 ML and 0.46 ML, respectively, the clusters are observed to wet the oxide support. The $Cu_{12}Pt_1H_6$ structure occupies an ellipsoidal-like space with a long side of 8.2 Å and a short side of 4.88 Å,

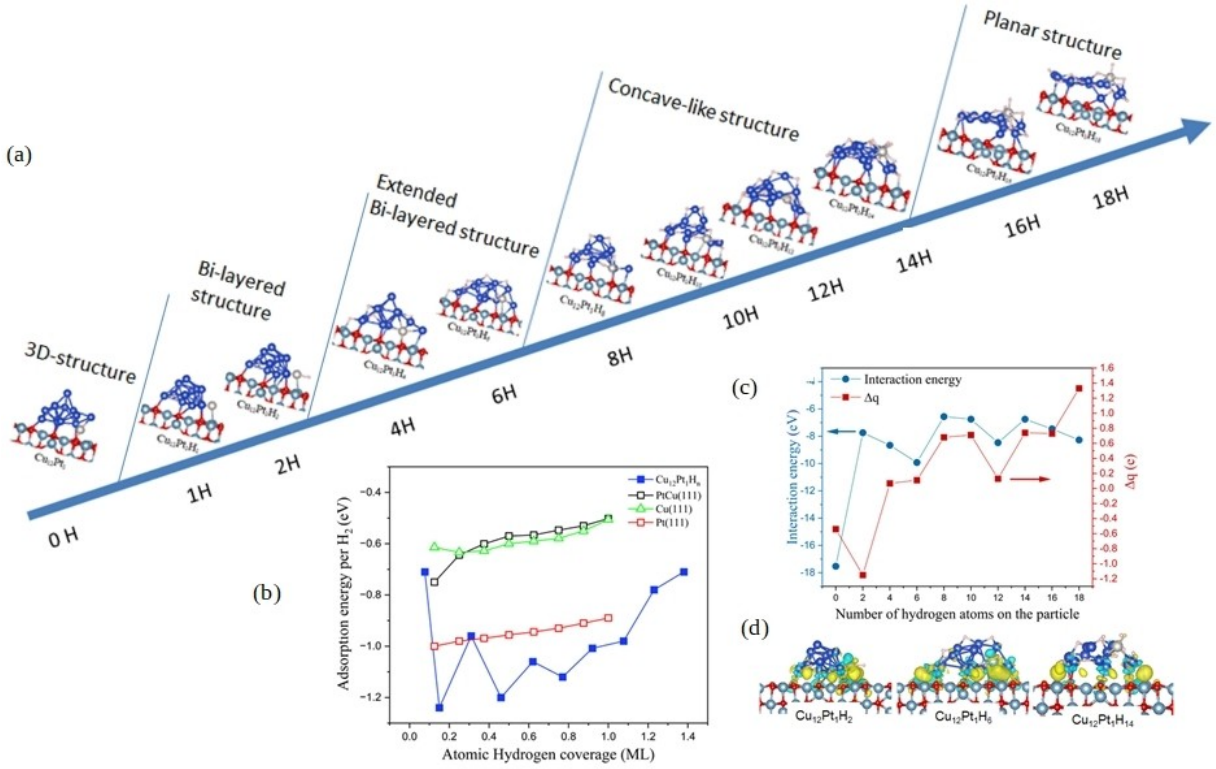

Figure 4. (a) Illustration of the morphological changes of the $Cu_{12}Pt_1/\gamma\text{-}Al_2O_3$ system in presence of increasing number of hydrogen atoms. Dark blue, light blue, red and white balls represent Cu, Al, O and Pt atoms, respectively. The small white balls represent adsorbed H atoms. (b) DFT calculated average adsorption energy values (in eV), plotted against hydrogen coverage (in ML) on $Cu_{12}Pt_1/\gamma\text{-}Al_2O_3$. The calculated adsorption energies of hydrogen on Pt(111), PtCu(111) and Cu(111) are also presented. (c) Evolution of the interaction energy between the alumina support and the hydrogenated $Cu_{12}Pt_1$ clusters and the Bader charge transfer from alumina surface to $Cu_{12}Pt_1H_n$ cluster. (d) Charge density difference $\Delta\rho = \rho(Cu_{12}Pt_1H_n/\gamma\text{-}Al_2O_3) - \rho(\gamma\text{-}Al_2O_3) - \rho(Cu_{12}Pt_1H_n)$ for n = 2, n = 6 and n = 14. $\Delta\rho$ is illustrated by iso-surfaces bounding regions of electron accumulation at $+0.0035$ e/Å^3 (yellow) and electron depletion at -0.0035 e/Å^3 (cyan). Positive $\Delta\rho$ means that the cluster has gained some electrons.

corresponding to an occupied area of approximately 30 Å^2. This area is almost twice as high as the occupied space of the pristine 3D cluster structure. In the meanwhile, the distance of the Pt atom to the support is found to increase compared to the free-hydrogen cluster. Specifically, the Pt–O and Pt–Al bindings increase from 2.12 Å and 2.45 Å to 2.99 Å and 2.66 Å in the $Cu_{12}Pt_1$@interface and $Cu_{12}Pt_1H_6$ structures, respectively. Moreover, as the hydrogen coverage increases, the single Pt atom diffuses from the interface site to the underside of the cluster and binds six Cu atoms with an average bonding length of 2.55 Å.

The third phase of morphological changes occurs within a coverage range between 0.61 ML and 1.08 ML. During this phase, the cluster undergoes shape evolution and adopts a concave-like structure, with one hydrogenated Cu atom formed on the top of the bell. Throughout the dynamics, the single Pt atom is observed to progressively move away from the oxide support, while remaining positioned beneath the Cu cluster. In the $Cu_{12}Pt_1H_{12}$ structure, the Pt atom is situated at a distance of 3 Å from the support. Subsequently, the concave structure is achieved at a coverage of 1.08 ML (14 H atoms), with the Pt single atom located on the upper layer of the cluster, interacting with five hydrogen atoms (one on top and four on the Cu–Pt bridge sites). The binding lengths of Pt–O and Pt–Al in this structure are found to be 4.16 Å and 4.12 Å, respectively.

In the fourth phase with hydrogen coverage above 1.08 ML, the cluster undergoes a transition toward a planar-like hydrogenated Cu structure. The dimensions of the planar $Cu_{12}Pt_1H_{18}$ structure (coverage of 1.38 ML) are 5.56 Å in width and 9.32 Å in length. In this highly hydrogenated cluster, the Pt atom interacts with six hydrogen atoms (four on the bridge Pt–Cu sites with $d_{Pt\text{-}H} = 1.68$ Å and two on the top site with $d_{Pt\text{-}H} = 1.59$ Å).

Effect of Hydrogen on the $Cu_{12}Pt_1$ interaction with the Support

Figure 4c reports the evolution of the interaction energy between the $Cu_{12}Pt_1H_n$ clusters and the alumina support, as well as the Bader charge transfers. A decrease in overall interaction energy with increasing hydrogen coverage is revealed, indicating a gradual weakening of the covalent metal-support interaction. The most significant evolution occurs between 0 and 0.15 ML of hydrogen coverage, where the interaction energy of the hydrogenated cluster decreases by more than 40% compared to the bare cluster. The Bader charge analysis predicts a charge transfer from the alumina surface to the $Cu_{12}Pt_1H_n$ cluster increasing with

higher hydrogen coverage. Interestingly, while the $Cu_{12}Pt_1$ and $Cu_{12}Pt_1H_2$ clusters are negatively charged, indicating electron density transfer to the support, the direction of charge transfer shifts with increasing hydrogen coverage. At hydrogen coverages of 0.30 ML and 0.46 ML, the entire cluster approaches a state of near neutrality, but then the charge difference becomes positive for increasing hydrogen coverage.

Finally, the charge density difference, illustrated in Figure 4d, reveals two significant peaks of electron accumulation at the cluster-alumina interface. Simultaneously, a more pronounced depletion of charge is observed in the cluster, particularly well above the interface, and this depletion intensifies with the increasing hydrogen coverage in line with the weakening of the cluster-support interaction.

Thermodynamics and Predicted Reactivity

Figure 5 depicts the (pH_2, T) phase diagram for $Cu_{12}Pt_1H_n/Al_2O_3$ (100), encompassing a pressure range from 1×10^{-16} to 1 bar and a temperature range from 0 to 1000 K. The phase diagram of the supported $Cu_{12}Pt_1$ cluster reveals limited ranges of stable hydrogen coverages, suggesting abrupt transitions from zero coverage to 1.08 ML. At the experimental temperature of 723 K for PDH reactions, and under pressure lower than10^{-3} bar, the free hydrogen $Cu_{12}Pt_1/Al_2O_3$ (100) system is predicted to be stable. As the pressure increases, the system evolves from bare surface to a bilayer structure (0.15 ML) and then, to a concave-like structure at 0.77 ML of hydrogen coverage. This indicates the cluster propensity to form hydride at lower temperature and/or when exposed to high hydrogen pressure.

The dominant features of the thermodynamic phase diagram for hydrogen adsorption on the supported $Cu_{12}Pt_1$ cluster indicate five stable phases at: 0 ML (0H), 0.15 ML (2H), 0.46 ML (6H), 0.77 ML (10H), and 1.08 ML (14H). Note that the stable phase at 0.46 ML only appears within a small window of temperature (215 K–245 K) and for pressure lower than 10^{-6} bar. Under laboratory pressure conditions of 10^{-2} bar, the stability of these five distinct phases can be described as follows: (i) at low temperatures up to approximately 350 K, the most stable phase is the concave structure with a coverage of 1.08 ML of atomic hydrogen; (ii) within the temperature range of 350 K to 600 K, the stable phase is a concave like structure with hydrogen coverage of 0.77 ML; (iii) in the temperature range between 600 K and 850 K, the stable phase is the bilayered structure covered by 0.15 ML of atomic hydrogen; (iv) finally, above 850 K, the clean $Cu_{12}Pt_1$ cluster becomes thermodynamically stable.

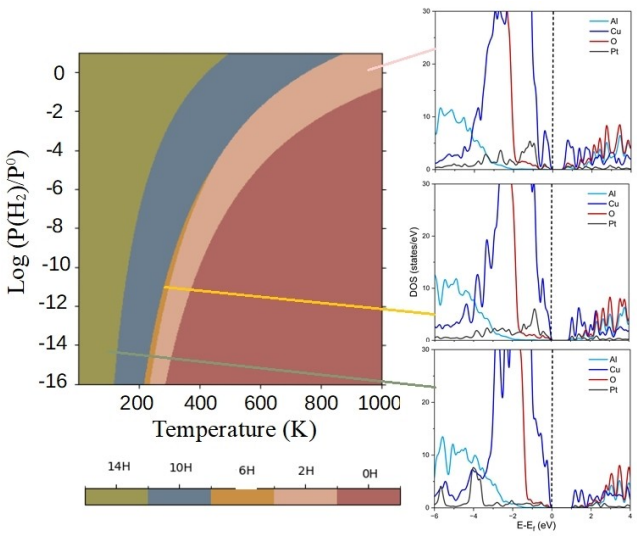

Figure 5. Thermodynamic phase diagram of the stability and the projected density of states (PDOS) of different elements for 0 ML, 0.15 ML (2H), 0.46 ML (6H), 0.77 ML (10H) and 1.08 ML (14H) of H coverage.

Figure 5 also shows PDOS of various elements for hydrogen adsorption on supported $Cu_{12}Pt_1$ cluster at coverages of 0.15 ML, 0.46 ML and 1.08 ML. The results indicate that the occupancy of the Cu 3*d* valence states close to the Fermi level remains significant, which suggests a heightened intrinsic reactivity of the metallic sites. Interestingly, the adsorption of hydrogen induces a gap opening, which increases from 0.52 eV for 2 adsorbed hydrogen (0.15 ML) to 0.93 eV and 0.99 eV for 6 (0.46 ML) and 14 (1.08 ML) adsorbed hydrogen, respectively.The appearance of the band gap at the Fermi level is associated with a more localized nature of the electronic states, which may alter the catalytic performance of the Pt–Cu cluster. This trend is consistent with the DFT results of $Pt_{13}H_n$ clusters supported on γ-Al_2O_3 (100) surface[37] and recent resonant inelastic X-ray scattering (RIXS) experiments.[38]

Conclusions

In conclusion, this study offers valuable insights into the stability, reactivity, and morphological evolution of $Cu_{12}Pt_1$ single atom alloy (SAA) clusters supported on alumina surfaces. Through a combination of density functional theory calculations and ab-initio molecular dynamics simulations, we have explored the dynamic interactions between Pt single atoms, Cu clusters, hydrogen, and the alumina support. Our findings reveal the significant influence of hydrogen coverage on the cluster's structural evolution, charge transfer, and metal-support interaction. Notably, we observed a gradual weakening of the covalent metal-support interaction with increasing hydrogen coverage, alongside a shift in the direction of charge transfer. Furthermore, we highlight the importance of considering environmental factors, such as gas environments and oxide supports, which can significantly affect the stability and reactivity of supported clusters. By providing atomic-scale insights, this work contributes to the fundamental understanding of Pt/Cu SAA cluster structural and electronic property evolution and paves the way for the design of novel catalysts with enhanced performance for various catalytic applications.

Theoretical Details

DFT calculations within periodic boundary conditions were performed with the Vienna Ab initio Simulation Package

(VASP),[39,40] using plane waves to solve the Kohn–Sham equations and the generalized gradient approximation as proposed by Perdew-Burke-Ernzerhof (PBE) for the exchange-correlation functional.[41] A kinetic energy cut-off of 400 eV was employed for expanding the plane waves, and the representation of core electrons was accomplished using the projected augmented wave method (PAW).[42] The van der Waals contributions were described with the semi-empirical Grimme DFT–D3 approach.[43] The convergence threshold for the total electronic energy was set to10^{-6} eV, and all structural configurations were iteratively optimized until atomic forces enabling relaxation were below 0.02 eV/Å. A Gaussian broadening technique with a σ value of 0.02 eV was applied to the $Cu_{12}Pt_1H_n$ clusters on the support. The evaluation of charge transfer was conducted using Bader charge analysis[44,45] at the same theoretical level.

To achieve the most stable configurations for various forms of Cu_{13}/Al_2O_3, $Cu_{12}Pt_1/Al_2O_3$, and hydrogen adsorption, a theoretical method consisted of a two-phase procedure was employed. In the initial phase, sets of geometries were fine-tuned using static DFT calculations to establish the optimal structures. Following this, the refined structures underwent equilibration using velocity-scaled AIMD simulations with the Born-Oppenheimer MD approach at 723 K (the standard reaction temperature for PDH reaction). This process was executed with a time-step of 5 fs and repeated over 2000 iterations. In the case of pure Cu_{13}/Al_2O_3 system (Figure S1), AIMD trajectories were prolonged to 4000 steps. As depicted in Figure S2, competitive arrangements were derived from the AIMD simulations with the lowest potential energy and subsequently cooled to 0 K through standard DFT geometry. The most stable quenched structures acquired from the AIMD simulations were employed to forecast the thermodynamic diagram, as elaborated in Reference.[21] This method, which integrates velocity-scaled molecular dynamics, quenching, and subsequent thermodynamic calculations using the harmonic approximation, has proven to be effective and resilient in studies involving platinum and platinum-tin clusters supported on alumina, encompassing diverse adsorbates.[10,20,45–47]

The structures of Cu_{13} and $Cu_{12}Pt_1$ clusters supported on alumina surface were constructed using the γ-Al_2O_3(100) surface model developed by Digne *et al.*.[48,49] This model represents the dehydrated surface under a wide array of significant operational conditions, encompassing various temperatures and partial pressures of water. The cell dimensions measure 16.71×16.79×25.80 $Å^3$, with γ-Al_2O_3 slab of 7.2 Å thickness along the z-axis. Each repetitively identical slab is adequately spaced from one another by a vacuum region of 20 Å. Let us note that according to Digne et al. [49] the considered alumina (100) surface is totally dehydrated above temperature of 600 K.

To study these systems, the sampling of Brillouin zones was executed using the Monkhorst-Pack approach[50] at the Γ point. In all calculations, a dipole correction was introduced to the overall electronic energy along the direction perpendicular to the slabs. During all processes of geometry optimization and AIMD simulations, complete relaxation was applied to the two uppermost alumina layers as well as all the cluster atoms, while the two lower alumina layers were held fixed.

The adsorption energy of one hydrogen atom on $Cu_{12}Pt$ clusters, is defined by Eq.(1):

$$E_{ads} = [E_{Cu12Pt1Hn/Al2O3} - E_{Cu12Pt1/Al2O3} - 1/2(E_{H2})] \quad (1)$$

When considering $Cu_{12}Pt_1$ clusters adorned with multiple hydrogen atoms, the mean co-adsorption energy per H_2 molecule is determined using Eq. (2) linked to the concurrent dissociative adsorption of several hydrogen molecules.

$$E_{coads} = 2/n\ [E_{Cu12Pt1Hn/Al2O3} - E_{Cu12Pt1/Al2O3} - n/2(E_{H2})] \quad (2)$$

In accordance with the chemical equation provided in Eq. (3):

$$Cu_{12}Pt_1/Al_2O_3 + n/2H_2 = Cu_{12}Pt_1H_n/Al_2O_3 \quad (3)$$

Here, n indicates the quantity of hydrogen atoms adsorbed within each cell of the $Cu_{12}Pt_1/\gamma\text{-}Al_2O_3$ system. The terms $E_{Cu12Pt1Hn/Al2O3}$ and $E_{Cu12Pt1/Al2O3}$ represent the total electronic energies of the studied system with and without adsorbed n hydrogen atoms, respectively. The energy of H_2 (E_{H2}) was computed by introducing an H_2 molecule into a symmetric box of size 12×12×12 $Å^3$ and subsequently conducting non-spin-polarized calculations.

The interaction energy between the support and the $Cu_{12}Pt_1$ cluster was calculated using Eq. (4):

$$E_{inter} = E_{Cu12Pt1Hn/Al2O3} - E^*_{Cu12Pt1Hn} - E^*_{Al2O3} \quad (4)$$

Here, $E_{Cu12Pt1Hn/Al2O3}$ represents the overall electronic energy of the supported configurations obtained through geometry optimization computations. $E^*_{Cu12Pt1Hn}$ and E^*_{Al2O3} represent the total electronic energies achieved *via* single-point calculations for the individual cluster and support systems, considering the geometries of the supported configuration. This energy pertains to the chemical bonding in the absence of any deformation energies of the individual components.

Constructing the (P_{H2}, T) phase diagram involves deriving adsorption entropies and enthalpies from DFT-optimized structures and conducting harmonic frequency calculations accordingly. The most stable structure achieved for each coverage underwent harmonic vibrational analysis with a displacement of ±0.01 Å in every direction for all relaxed atoms within the cell. Subsequently, the Hessian matrix was computed using the finite-difference technique and subjected to diagonalization to anticipate harmonic normal modes and their corresponding vibrations. In the case of condensed phases, a total of 3 N^{-3} real vibrational frequencies were considered to assess the thermal and entropy contributions. Comprehensive explanations of the free energy calculations for every system can be found in ref. [38]. The construction of the thermodynamic diagrams relies on the hydrogen-adsorption free energy ΔG adsorption, as outlined in Eq. (5). The coverage domains depicted on the different thermodynamic diagrams correspond to the lowest obtained free energy values at (P_{H2}, T), as determined by:

$$\Delta G_{ads}\ (P_{H2},\ T,\ \theta_{H2}) = G_{Cu12Pt1Hn}(T,\ \theta_{H2}) - G_{Cu12Pt1}(T) - n/2\ G_{H2}\ (P_{H2},\ T) \quad (5)$$

Supporting Information

Structures of supported clusters, potential energy evolution along AIMD trajectories, and DFT H-adsorption energies. Link to the SI file

Acknowledgements

This work pertains to the French government program "Investissements d'Avenir" (EUR INTREE, grant number ANR-18-EURE-0010). The authors gratefully acknowledge the French National Agency for Research (ANR), grant number ANR-21-CE07-0029 (BINOME project). This work was performed using HPC resources from GENCI-IDRIS (Grant 2023-[A0130807369]).

H.G. would like to thank Dr. Céline Chizallet and Dr. P. Raybaud for providing γ-alumina surface model and for insightful discussions regarding the results.

Conflict of Interests

The authors declare no conflict of interest.

Data Availability Statement

The data that support the findings of this study are available from the corresponding author upon reasonable request.

Keywords: SAA catalysts · Hydrogen effect · Cluster · DFT · AIMD

[1] E. C. Tyo, S. Vajda, *Nat. Nanotechnol.* **2015**, *10*, 577–588.
[2] M. Boronat, A. Leyva-Pérez, A. Corma, *Acc. Chem. Res.* **2014**, *47*, 834–844.
[3] P. Concepción, M. Boronat, S. García-García, E. Fernández, A. Corma, *ACS Catal.* **2017**, *7*, 3560–3568.
[4] P. Maity, S. Yamazoe, T. Tsukuda, *ACS Catal.* **2013**, *3*, 182–185.
[5] J. Oliver-Messeguer, L. Liu, S. García-García, C. Canós-Giménez, I. Domínguez, R. Gavara, A. Doménech-Carbó, P. Concepción, A. Leyva-Pérez, A. Corma, *J. Am. Chem. Soc.* **2015**, *137*, 3894–3900.
[6] K. Yamamoto, T. Imaoka, W.-J. Chun, O. Enoki, H. Katoh, M. Takenaga, A. Sonoi, *Nat. Chem.* **2009**, *1*, 397–402.
[7] S. Vajda, M. J. Pellin, J. P. Greeley, C. L. Marshall, L. A. Curtiss, G. A. Ballentine, J. W. Elam, S. Catillon-Mucherie, P. C. Redfern, F. Mehmood, P. Zapol, *Nat. Mater.* **2009**, *8*, 213–216.
[8] J. Rodriguez, *Surf. Sci. Rep.* **1996**, *24*, 223–287.
[9] S. Kim, J. Lauterbach, E. Sasmaz, *ACS Catal.* **2021**, *11*, 8247–8260.
[10] S. Sun, G. Sun, C. Pei, Z.-J. Zhao, J. Gong, *J. Phys. Chem. C* **2021**, *125*, 18708–18716.
[11] S. Zhang, R. Wang, X. Zhang, H. Zhao, *RSC Adv.* **2024**, *14*, 3936–3951.
[12] A. Han, J. Zhang, W. Sun, W. Chen, S. Zhang, Y. Han, Q. Feng, L. Zheng, L. Gu, C. Chen, Q. Peng, D. Wang, Y. Li, *Nat. Commun.* **2019**, *10*, 3787.
[13] Y. Nakaya, J. Hirayama, S. Yamazoe, K.-I. Shimizu, S. Furukawa, *Nat. Commun.* **2020**, *11*, 2838.
[14] S. Kumari, P. Sautet, *J. Mater. Chem. A* **2021**, *9*, 15724–15733.
[15] M. D. Marcinkowski, M. T. Darby, J. Liu, J. M. Wimble, F. R. Lucci, S. Lee, A. Michaelides, M. Flytzani-Stephanopoulos, M. Stamatakis, E. C. H. Sykes, *Nat. Chem.* **2018**, *10*, 325–332.
[16] Z. Ma, Z. Wu, J. T. Miller, *Catalysis, Structure, Reactivity.* **2017**, *3*, 43–53.
[17] G. Sun, Z.-J. Zhao, R. Mu, S. Zha, L. Li, S. Chen, K. Zang, J. Luo, Z. Li, S. C. Purdy, A. J. Kropf, J. T. Miller, L. Zeng, J. Gong, *Nat. Commun.* **2018**, *9*, 4454.
[18] S. Zha, G. Sun, T. Wu, J. Zhao, Z.-J. Zhao, J. Gong, *Chem. Sci.* **2018**, *9*, 3925–3931.
[19] A. Gorczyca, P. Raybaud, V. Moizan, Y. Joly, C. Chizallet, *ChemCatChem.* **2019**, *11*, 3941–3951.
[20] Q. Wang, A. Nassereddine, D. Loffreda, C. Ricolleau, D. Alloyeau, C. Louis, L. Delannoy, J. Nelayah, H. Guesmi, *Faraday Discuss.* **2023**, *242*, 375–388.
[21] M. Shahrokhi, C. Chizallet, D. Loffreda, P. Raybaud, *ChemCatChem.* **2022**, *14*, e202201089.
[22] N. Dimitrova, M. Dhifallah, T. Mineva, T. Boiadjieva-Scherzer, H. Guesmi, J. Georgieva, *RSC Adv.* **2019**, *9*, 2073–2080.
[23] J. Wisniewska, H. Guesmi, M. Ziolek, F. Tielens, *J. Alloys Compd.* **2019**, *770*, 934–941.
[24] Q. Wang, B. Zhu, F. Tielens, D. Tichit, H. Guesmi, *Appl. Surf. Sci.* **2021**, *548*, 149217.
[25] Q. Wang, D. Tichit, F. Meunier, H. Guesmi, *J. Phys. Chem. C* **2020**, *124*, 9979–9989.
[26] H. Guesmi, *Gold Bull.* **2013**, *46*, 213–219.
[27] D. K. Limbu, P. Biswas, *J. Phys. Conf. Ser.* **2017**, *921*, 012010.
[28] J. P. K. Doye, D. J. Wales, *New J. Chem.* **1998**, *22*, 733–744.
[29] J. Oviedo, R. E. Palmer, *J. Chem. Phys.* **2002**, *117*, 9548–9551.
[30] C. M. Chang, M. Y. Chou, *Phys. Rev. Lett.* **2004**, *93*, 133401.
[31] C. Kittel, Introduction to Solid State Physics, Wiley, **2004**.
[32] B. Hammer, J. K. Nørskov, *Surf. Sci.* **1995**, *343*, 211–220.
[33] A. Nilsson, L. G. M. Pettersson, J. K. Nørskov, in *Chemical Bonding at Surfaces and Interfaces*, *Vol.*, Elsevier Science **2007**.
[34] G. Sun, A. N. Alexandrova, P. Sautet, *J. Chem. Phys.* **2019**, *151*, 194703.
[35] K. Gu, S. Lin, *Angew. Chem. Int. Ed.* **2023**, *62*, e202312796.
[36] G. Feng, M. V. Ganduglia-Pirovano, C.-F. Huo, J. Sauer, *J. Phys. Chem. C* **2018**, *122*, 18445–18455.
[37] C. Mager-Maury, G. Bonnard, C. Chizallet, P. Sautet, P. Raybaud, *ChemCatChem.* **2011**, *3*, 200–207.
[38] J. Singh, R. C. Nelson, B. C. Vicente, S. L. Scott, J. A. van Bokhoven, *Phys. Chem. Chem. Phys.* **2010**, *12*, 5668–5677.
[39] G. Kresse, J. Furthmüller, *Phys. Rev. B* **1996**, *54*, 11169–11186.
[40] G. Kresse, J. Furthmüller, *Comput. Mater. Sci.* **1996**, *6*, 15–50.
[41] J. P. Perdew, K. Burke, M. Ernzerhof, *Phys. Rev. Lett.* **1996**, *77*, 3865–3868.
[42] G. Kresse, D. Joubert, *Phys. Rev. B* **1999**, *59*, 1758–1775.
[43] S. Grimme, J. Antony, S. Ehrlich, H. Krieg, *J. Chem. Phys.* **2010**, *132*.
[44] E. Sanville, S. D. Kenny, R. Smith, G. Henkelman, *J. Comput. Chem.* **2007**, *28*, 899–908.
[45] G. Henkelman, A. Arnaldsson, H. Jónsson, *Comput. Mater. Sci.* **2006**, *36*, 354–360.
[46] W. Zhao, C. Chizallet, P. Sautet, P. Raybaud, *J. Catal.* **2019**, *370*, 118–129.
[47] A. Sangnier, M. Matrat, A. Nicolle, C. Dujardin, C. Chizallet, *J. Phys. Chem. C* **2018**, *122*, 26974–26986.
[48] M. Digne, P. Sautet, P. Raybaud, P. Euzen, H. Toulhoat, *J. Catal.* **2002**, *211*, 1–5.
[49] M. Digne, P. Sautet, P. Raybaud, P. Euzen, H. Toulhoat, *J. Catal.* **2004**, *226*, 54–68.
[50] H. J. Monkhorst, J. D. Pack, *Phys. Rev. B* **1976**, *13*, 5188–5192.

Manuscript received: March 24, 2024
Revised manuscript received: May 6, 2024
Accepted manuscript online: June 4, 2024
Version of record online: July 6, 2024